RESEARCH ARTICLE

Cardiac lipotoxicity and fibrosis underlie impaired contractility in a mouse model of metabolic dysfunction-associated steatotic liver disease

Olufunto O. Badmus 🄳 | Alexandre A. da Silva 🄳 | Xuan Li | Lucy C. Taylor 🄳 | Jennifer R. Greer | Andrew R. Wasson | Karis E. McGowan | Parth R. Patel | David E. Stec 🄳

Department of Physiology & Biophysics, Cardiorenal, and Metabolic Diseases Research Center, Cardiovascular-Renal Research Center, University of Mississippi Medical Center, Jackson, Mississippi, USA

Correspondence
Olufunto O. Badmus, Department of Physiology & Biophysics, Cardiorenal, and Metabolic Diseases Research Center, Cardiovascular-Renal Research Center, University of Mississippi Medical Center, 2500 North State Street, Jackson, MS 39216-4505, USA.
Email: obadmus@umc.edu

Abstract

The leading cause of death among patients with metabolic dysfunction-associated steatotic liver disease (MASLD) is cardiovascular disease. A significant percentage of MASLD patients develop heart failure driven by functional and structural alterations in the heart. Previously, we observed cardiac dysfunction in hepatocyte-specific peroxisome proliferator-activated receptor alpha knockout ($Ppara^{HepKO}$), a mouse model that exhibits hepatic steatosis independent of obesity and insulin resistance. The goal of the present study was to determine mechanisms that underlie hepatic steatosis-induced cardiac dysfunction in $Ppara^{HepKO}$ mice. Experiments were performed in 30-week-old $Ppara^{HepKO}$ and littermate control mice fed regular chow. We observed decreased cardiomyocyte contractility (0.17 ± 0.02 vs. $0.24 \pm 0.02 \mu m$, $p < 0.05$), increased cardiac triglyceride content (0.96 ± 0.13 vs. $0.68 \pm 0.06 mM$, $p < 0.05$), collagen type 1 (4.65 ± 0.25 vs. $0.31 \pm 0.01 AU$, $p < 0.001$), and collagen type 3 deposition (1.32 ± 0.46 vs. $0.05 \pm 0.03 AU$, $p < 0.05$). These changes were associated with increased apoptosis as indicated by terminal deoxynucleotidyl transferase dUTP nick end labeling staining (30.9 ± 4.7 vs. $13.1 \pm 0.8\%$, $p < 0.006$) and western blots showing increased cleaved caspase-3 (0.27 ± 0.006 vs. $0.08 \pm 0.01 AU$, $p < 0.003$) and pro-caspase-3 (5.4 ± 1.5 vs. $0.5 \pm 0.3 AU$, $p < 0.02$), B-cell lymphoma protein 2-associated X (0.68 ± 0.07 vs. $0.04 \pm 0.04 AU$, $p < 0.001$), and reduced B-cell lymphoma protein 2 (0.29 ± 0.01 vs. $1.47 \pm 0.54 AU$, $p < 0.05$). We further observed elevated circulating

---

Abbreviations: ANP, atrial natriuretic peptide; ATP, adenosine triphosphate; BAX, B-cell lymphoma protein 2-associated X; BCL-2, B-cell lymphoma protein 2; BDH1, D-β-hydroxybutyrate dehydrogenase I; BHOB, beta hydroxybutyrate; BNP, B-type natriuretic peptide; cDNA, complementary deoxyribonucleic acid; COL1A1, collagen type I alpha 1; COL3A1, collagen type III alpha 1; CVD, cardiovascular disease; HSP90, heat shock protein 90; MASLD, metabolic dysfunction-associated steatotic liver disease; mRNA, messenger ribonucleic acid; PCR, polymerase chain reaction; Ppara$^{fl/fl}$, hepatocyte-specific peroxisome proliferator-activated receptor alpha flox/flox; Ppara^{HepKO}, hepatocyte-specific peroxisome proliferator-activated receptor alpha knockout; RER, respiratory exchange ratio; SEM, standard error of mean; TUNEL, terminal deoxynucleotidyl transferase dUTP nick end labeling; VCO$_2$, volume of carbon dioxide production; VO$_{2max}$, maximum volume of oxygen consumption.

natriuretic peptides and exercise intolerance in $Ppara^{HepKO}$ mice when compared to controls. Our data demonstrated that lipotoxicity, and fibrosis underlie cardiac dysfunction in MASLD.

1 | INTRODUCTION

Cardiovascular disease (CVD) remains a serious complication of nonalcoholic fatty liver disease (NAFLD) accounting for more than 40% of mortality in NAFLD patients.[1] NAFLD is associated with increased risk of coronary artery disease, heart failure, and valvular dysfunction.[2] The exact mechanism by which NAFLD drives CVD is not fully understood given that NAFLD is often coupled with obesity, insulin resistance, and dyslipidemia; so that the contribution of NAFLD to CVD is confounded by these accompanying risk factors. In addition, due to the importance of increased incidence of hepatic steatosis associated with obesity and metabolic syndrome, a new nomenclature of metabolic dysfunction-associated steatotic liver disease (MASLD) was recently adopted.[3] Several mechanisms such as inflammation, oxidative stress, insulin resistance, and hypobilirubinemia have been described to link MASLD with CVD.[4–6]

In MASLD patients, there is increased availability of circulating triglyceride and free fatty acids, and this can lead to ectopic lipid accumulation in non-adipose tissues including the heart, kidney, and blood vessels.[7,8] Under normal circumstances, the heart consumes large amount of fatty acids to constantly generate adenosine triphosphate (ATP) to supply the high energy demand of the heart. At the same time, lipid storage within the myocardium is tightly regulated, and the physiological balance between cardiac lipid uptake and fatty acid oxidation prevents cardiac lipid overload in a healthy heart.[9] However, lipids become harmful when accumulated in excess, contributing to altered cardiac structure and function. There is growing evidence that diseased conditions associated with disorders of lipid metabolism can result in lipid accumulation in the heart.[10,11] Excess cardiac lipid accumulation has been associated with the initiation of apoptotic cascades in cardiomyocytes, a pathophysiological progression called cardiac lipotoxicity that can lead to myocardial dysfunction.[10,12] Notably, emerging findings have revealed that cardiac lipotoxicity is a vital risk factor for development of heart failure with preserved ejection fraction often observed in patients with MASLD.[13]

In a previous study from our lab, we characterized the cardiovascular phenotype of hepatocyte-specific peroxisome proliferator-activated receptor alpha knockout ($Ppara^{HepKO}$). These mice exhibit hepatic steatosis in the absence of obesity, insulin resistance, and alterations in plasma triglycerides and lipids.[13] We observed that the $Ppara^{HepKO}$ mice are also hypertensive, and exhibit left ventricular remodeling with altered cardiac function and vascular stiffness.[13] Thus, this mouse model provides an opportunity to examine the impact of MASLD on the cardiovascular system, including the heart, in the absence of confounding effects of obesity and obesity-associated metabolic abnormalities. The present study was designed to determine the mechanisms responsible for the alterations in cardiac function in $Ppara^{HepKO}$ mice. We observed in the current study that $Ppara^{HepKO}$ mice exhibit increased cardiac steatosis, associated with increased apoptosis, cardiomyocyte contractile dysfunction, excess cardiac collagen deposition, elevated expression of natriuretic peptides, and decreased exercise capacity.

2 | RESEARCH DESIGN AND METHODS

2.1 | Animals

The experimental procedures and protocols of this study were approved by the Institutional Animal Care and Use Committee of the University of Mississippi Medical Center in accordance with the *NIH Guide for the Care and Use of Laboratory Animals*. All procedures conformed to the National Institutes of Health Guide for the Care and Use of Laboratory Animals and. Animals were housed in a temperature-controlled environment with a 12–12 h dark–light cycle under standard temperatures between 24 and 25°C with free access to food and water ad libitum. $Ppara^{HepKO}$ and hepatocyte-specific peroxisome proliferator-activated receptor alpha flox/flox ($Ppara^{fl/fl}$) mice were bred in our colony at the

University of Mississippi Medical Center as previously described.[13,14] The standard mouse chow consisted of 17% fat (Teklad diet, #8604, Harland Laboratories, Inc., Indianapolis, IN). Studies were performed on 30-week-old male mice. Investigators were blinded to the genotypes of the mice at the time of experimentation. Mice were fasted 8 h from early morning to afternoon prior to euthanasia via isoflurane anesthesia, and blood and tissues were collected and stored at −80°C for further analysis.

2.2 | Exercise tolerance test

At the end of experiments, the exercise capacity of mice was tested. Mice were initially trained to acclimatize to a 6-lane small animal treadmill (Columbus Instruments) for 2 days at 9 m/min for 5 min, before performing a graded maximal exercise endurance test. On the third day, mice were subjected to a graded exercise test on a modular single lane treadmill (Columbus instrument) connected to an OXYMAX/Comprehensive Lab Animal Monitoring System setup, to measure maximal oxygen consumption, volume of carbon dioxide production (VCO_2), and respiratory exchange ratio (RER) by indirect calorimetry to assess their aerobic capacity. The treadmill was set to an initial inclination of 5° and the following protocol was used until exhaustion (speed, duration, and grade): – (9 m/min, 2 min, and 5°), (12 m/min, 2 min, and 10°), (15 m/min, 2 min, and 15°), (18 m/min, 1 min, and 15°), (21 m/min, 1 min, and 15°), (23 m/min, 1 min, and 15°), (24 m/min, 1 min, and 15°), and (+1 m/min, each min thereafter, and 15°). Exhaustion (endpoint of exercise) was determined as an inability to maintain running speed and the mouse is repeatedly maintaining contact with the shock grid for ~5 s. Once mice ran to exhaustion, each mouse was immediately removed from the treadmill and blood lactate concentration was measured from tail vein blood samples using a lactate strip and meter (Nova Biomedical). Blood lactate concentration at rest was measured 2 days before the exercise test.

2.3 | Plasma and cardiac triglyceride measurements

Plasma and cardiac tissue triglyceride levels were measured using a colorimetric assay kit according to the manufacturer's guidelines (Triglyceride Assay Kit, Abcam, Cambridge, UK) as we have previously described.[14,15] Samples from individual mice were run in duplicate and averaged, and the averages of individual mice were then used to obtain group averages.

2.4 | Histology

Cardiac lipid contents were measured by Oil Red O staining of frozen tissue sections as previously described.[14,16] Cardiac collagen content was determined by picrosirius red staining of paraffin-embedded cardiac tissue sections as previously described.[17] Histological images of Oil Red O and picrosirius red stains were taken at 40× magnification of individual stained sections using a color brightfield camera of the BioTek Lionheart FX automated microscope, and their percentages were determined from each field using NIH ImageJ software. Sixteen measurements from four different sections per individual animal were averaged and the averages of individual mice were then used to obtain the group averages.

2.5 | TUNEL staining

Terminal deoxynucleotidyl transferase dUTP nick end labeling (TUNEL) staining was used to determine cardiac apoptosis. Formalin-fixed transverse ventricular slices were embedded in paraffin and cut into 4-μm serial sections that were used for TUNEL staining. TUNEL was performed with the In-Situ Cell Death Detection Kit (Roche Molecular Biochemicals) according to the manufacturer's instructions. After adding 50 ul of TUNEL reaction mixture followed by 50 μL of DAB substrate on sample, all nuclei were counterstained with hematoxylin. For each specimen, the number of TUNEL-positive myocytes and the number of total myocytes were counted in high-power brightfields using Mantra 2™ Quantitative Pathology Workstation. Approximately 2000 total myocytes were examined per section. The percentage of total myocytes that were TUNEL-positive (apoptotic index) was then calculated using the inForm analysis.

2.6 | Total RNA extraction, isolation, and real-time PCR analysis

Total RNA was extracted from mouse hearts using RNeasy Mini Kits (QIAGEN Inc., Austin, Texas) according to manufacturer's protocol and complementary deoxyribonucleic acid (cDNA) was synthesized using high-capacity cDNA reverse transcription kit (Applied Biosystems). This was used to assay the expressions of atrial natriuretic peptide (ANP) and B-type natriuretic peptide (BNP). Polymerase chain reaction (PCR) amplification of the cDNA was performed by quantitative real-time PCR using TrueAmp SYBR Green qPCR SuperMix (Alkali Scientific) for gene-specific primers (ANP: Ar-TACAGTGCGGTGTCCAACACAG/ Br-TGCTTCCTCAGTCTGCTCACTC; BNP: Ar-TCCT

AGCCAGTCTCCAGAGCAA/Br-GGTCCTTCAAGAG CTGTCTCTG; Eurofins Genomics LLC., Louisville, KY). Details of the thermocycling protocols used for this study have been previously reported.[14] Normalization was performed in separate reactions with primers to GAPDH.

2.7 | Western blotting

Western blots were performed on cardiac and liver samples (30 μg) as we previously described.[13,14,18] Membranes were incubated overnight at 4°C with the following antibodies: ANP (1:1000, Abcam, ab180649), BNP (1:1000, Santa Cruz Biotechnology, sc-271185), cleaved anti-caspase-3 (1:1000, Cell Signaling Technology, #9661), Pro-caspase-3 (1:1000, NovusBio, B-6), B-cell lymphoma protein 2 (BCl-2) (1:1000, Santa Cruz Biotechnology, sc-7382), B-cell lymphoma protein 2-associated X (BAX) (1:1000, Invitrogen, YB3837921), D-β-hydroxybutyrate dehydrogenase I (BDH1) (1:2000,15417, Thermofisher), and heat shock protein 90 (1:5000, Santa Cruz Biotechnology, sc-13119). After three washes in TBS+0.1% Tween 20, the membrane was incubated with an infrared donkey anti-goat (IRDye 800LI-COR Biosciences, 926-32214) or donkey anti-rabbit (IRDye 800LI-COR Biosciences, 926-32214) or goat anti-mouse (IRDye 680, LI-COR Biosciences, 926-68020) secondary antibody (LI-COR Biosciences) (1:2,000 dilution in TBS) for 2hrs at 4°C. Immunoreactivity was visualized and quantified by infrared scanning in the Odyssey system (LI-COR Biosciences).

2.8 | Cardiomyocyte isolation and contractility measurement

Cardiac myocytes were isolated as previously described.[19] The hearts were excised, aortas were cannulated and connected to a heart perfusion apparatus (Radnoti, CA). The heart was perfused with a Ca^{2+}-free based buffer (pH 7.2, 37°C) containing: 135 mmol/L NaCl, 4 mmol/L KCl, 1 mmol/L MgCl2, 10 mmol/L HEPES, 0.33 mmol/L NaH2PO4, 10 mmol/L glucose, 10 mmol/L 2,3-butanedione monoxime (Sigma; B0753), and 5 mmol/L taurine (Sigma; T0625) and bubbled with 95% O_2/5% CO_2. After 3–5 min of perfusion, the buffer was replaced with similar buffer containing 0.3 mg/g body weight collagenase D (Sigma Aldrich; 66505623), 0.4 mg/g body weight collagenase B (Sigma Aldrich; 63603623), and 0.05 mg/g body weight protease type XIV (Sigma Aldrich; 9036-06-0) dissolved in 25 mL perfusion buffer. After complete digestion of the heart (6–8 min), the hearts were removed from the apparatus, atria trimmed off, and ventricles gently minced to release individual myocytes. Extracellular Ca^{2+} at different concentrations of (0.06 mmol/L, 0.24 mmol/L, 0.6 mmol/L, and 1.2 mmol/L) was gradually added back to the cells at intervals of 15 min. Cardiomyocyte dimensions, contractile and relaxation function were measured using SoftEdgeMyocam system (IonOptix, Westwood, MA). Glass cover slips containing isolated cardiomyocytes were mounted in a chamber and stimulated with a supra-threshold voltage at a frequency of1Hz. Changes in sarcomere length and duration of shortening and relengthening were recorded. Approximately 20 contractile cycles were averaged for each cell. Data were analyzed using IonOptix SoftEdge Software (IonOptix, Westwood, MA, Ionoptix.com), and approximately 30 cardiomyocytes were analyzed from each of three mice per group.

2.9 | Statistical analysis

Data were analyzed with Prism 10 (GraphPad Software, San Diego, CA) using unpaired *t*-tests. Results are expressed as mean ± standard error of mean. Statistically significant differences were accepted at *p* values of 0.05 or smaller.

3 | RESULTS

3.1 | Ppara[HepKO] mice exhibit increased cardiac lipotoxicity, increased levels of apoptosis, and increased fibrosis

Oil Red O staining of heart sections revealed increased lipid accumulation in *Ppara*[HepKO] as compared to *Ppara*^{fl/fl} mice (Figure 1A). The levels of triglycerides were also significantly increased in the hearts of *Ppara*[HepKO] as compared to *Ppara*^{fl/fl} mice (Figure 1B). On the contrary, plasma triglycerides in *Ppara*[HepKO] mice did not show any significant changes compared to *Ppara*^{fl/fl} mice (Figure 1C). It is important to note that these are fasting measurements of plasma triglycerides. Next, the levels of cardiac apoptosis were determined with TUNEL staining of heart sections as well as by measuring several proteins involved in apoptosis. TUNEL staining of heart sections showed increased levels of apoptosis in *Ppara*[HepKO] versus *Ppara*^{fl/fl} mice (30.9 ± 4.7 vs. 13.1 ± 0.8%, $p < 0.006$) (Figure 2A). This was accompanied by elevated levels of the proapoptotic proteins cleaved caspase-3 and pro-caspase-3 (Figure 2B) and BAX (Figure 2C), and reduced levels of the antiapoptotic protein BCL-2 (Figure 2D). *Ppara*[HepKO] mice exhibited significantly increased picrosirius red staining compared to *Ppara*^{fl/fl} mice (Figure 3A). Western blot analysis revealed significantly elevated levels of collagen type I (Figure 3B) and collagen type 3 (Figure 3C) in hearts of *Ppara*[HepKO] compared with *Ppara*^{fl/fl} mice. These results demonstrate that *Ppara*[HepKO] mice on a normal diet develop cardiac lipotoxicity due to increased lipid accumulation and exhibit increased levels of cardiomyocyte apoptosis as well as increased fibrosis.
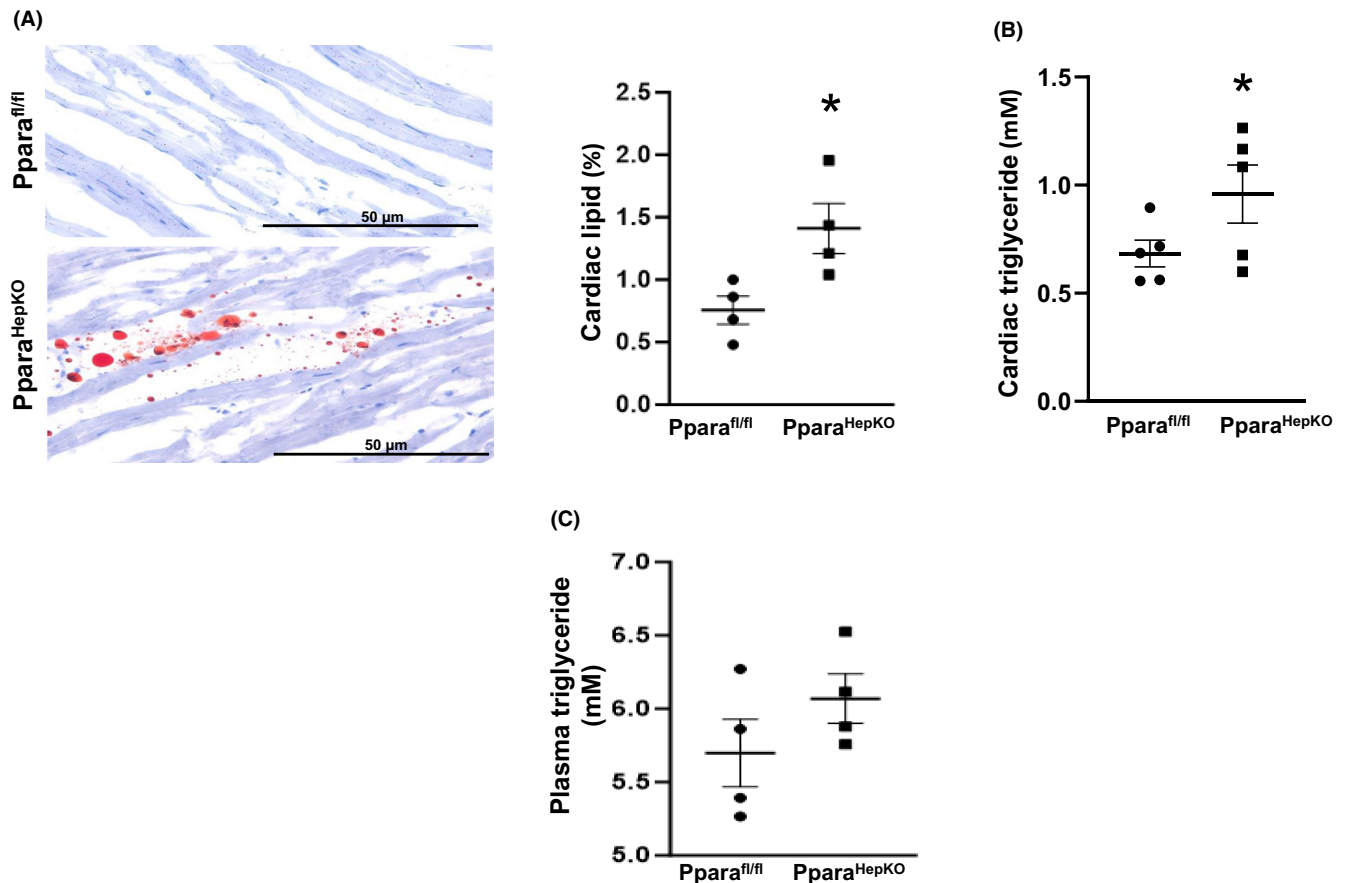
FIGURE 1 Cardiac lipid accumulation in *Ppara*^{HepKO} and *Ppara*^{fl/fl} mice. (A) Representative oil red O staining of cardiac tissue from *Ppara*^{HepKO} and floxed littermate controls (*Ppara*^{fl/fl}), and (B) cardiac triglyceride levels. (C) Plasma triglyceride levels. Values are expressed as means ± SEM; *$p < 0.05$ versus *Ppara*^{fl/fl}; $n = 4$–5/group. Scale bar = 50 μm. Ppara^{fl/fl}, hepatocyte-specific peroxisome proliferator-activated receptor alpha flox/flox; Ppara^{HepKO}, hepatocyte-specific peroxisome proliferator-activated receptor alpha knockout; SEM, standard error of mean.

3.2 | Decreased cardiomyocyte contractility in Ppara^{HepKO} mice

Cardiomyocytes were isolated from *Ppara*^{fl/fl} and *Ppara*^{HepKO} mice to determine sarcomere length and contractility. Figure 4A depicts a representative cardiac myocyte contractile trace from both *Ppara*^{fl/fl} and *Ppara*^{HepKO} mice. Compared to the *Ppara*^{fl/fl} mice, cardiac myocytes from *Ppara*^{HepKO} mice have significantly increased baseline sarcomere length (Figure 4B). In addition, cardiomyocytes from *Ppara*^{HepKO} mice show decreased peak sarcomere shortening (Figure 4C) and contraction velocity (Figure 4D), both reflective of decreased cardiomyocyte contractility in *Ppara*^{HepKO} mice. Furthermore, the time from baseline to peak shortening (Figure 4E), and time from peak to 50% relaxation (Figure 4F) were significantly increased in cardiomyocytes from *Ppara*^{HepKO} mice compared to the *Ppara*^{fl/fl} mice, indicating diminished contractile function and slowed relaxation in *Ppara*^{HepKO} mice.

3.3 | Elevated markers of heart failure and decreased levels of D-β-hydroxybutyrate dehydrogenase I in Ppara^{HepKO} mice

ANP and brain natriuretic peptide (BNP) are proteins synthesized in the heart and used as markers of heart failure. Cardiac messenger ribonucleic acid expression and protein levels of ANP and BNP (Figure 5A–C) were significantly elevated in *Ppara*^{HepKO} mice. Cardiac BDH1 protein levels were significantly reduced in *Ppara*^{HepKO} mice compared to the *Ppara*^{fl/fl} mice (Figure 5D).

3.4 | Reduced exercise tolerance and aerobic capacity in Ppara^{HepKO} mice

In order to determine the impact of the observed structural and functional changes in hearts of *Ppara*^{HepKO} mice, we exposed *Ppara*^{fl/fl} and *Ppara*^{HepKO} mice to an
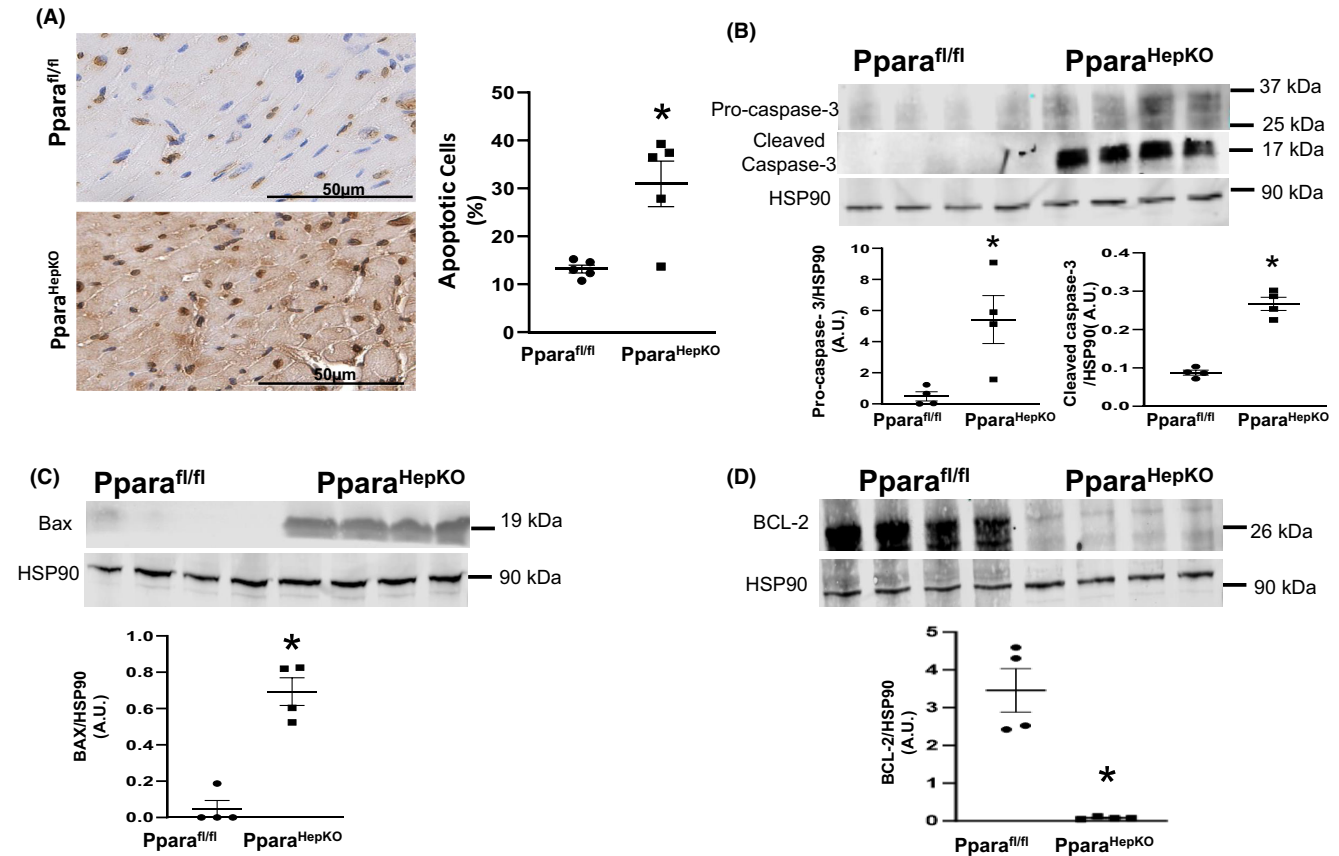
FIGURE 2 Cardiomyocyte apoptosis in *Ppara*[HepKO] and *Ppara*^{fl/fl} mice. (A) Representative TUNEL staining of cardiac tissue from *Ppara*[HepKO] and floxed littermate controls (*Ppara*^{fl/fl}), (B) Representative western blot of cardiac cleaved caspase −3 and pro-caspase-3 normalized to HSP90 levels, (C) cardiac BAX, and (D) cardiac BCL-2 in *Ppara*[HepKO] and *Ppara*^{fl/fl} mice. Values are expressed as means ± SEM; *$p < 0.05$ versus *Ppara*^{fl/fl}; (A) $n = 5$/group, (B–D); $n = 4$/group; Scale bar = 50 μm. BAX, B-cell lymphoma protein 2-associated X; BCL-2, B-cell lymphoma protein 2; HSP90, heat shock protein 90; Ppara^{fl/fl}, hepatocyte-specific peroxisome proliferator-activated receptor alpha flox/flox; Ppara[HepKO], hepatocyte-specific peroxisome proliferator-activated receptor alpha knockout; SEM, standard error of mean; TUNEL, terminal deoxynucleotidyl transferase dUTP nick end labeling.

exercise tolerance test to assess cardiovascular fitness. We also measured blood lactate levels before and after exercise as the lactate threshold is a good predictor of submaximal fitness. There was an increase in resting blood lactate levels in *Ppara*[HepKO] mice as compared to *Ppara*^{fl/fl} mice (Figure 6A), but no change in lactate levels after exercise (Figure 6B). Time until exhaustion during exercise (Figure 6C), as well as exercise performance were significantly decreased in *Ppara*[HepKO] mice compared to *Ppara*^{fl/fl} controls (Figure 6D). Also, maximum volume of oxygen consumption (VO[2max]) consumed during exercise was reduced in *Ppara*[HepKO] mice (Figure 6E), and RER of *Ppara*[HepKO] mice crossed the 1.0 mark at an earlier time point compared to *Ppara*^{fl/fl} mice, suggesting a more rapid shift from aerobic to anaerobic metabolism during exercise (Figure 6F).

4 | DISCUSSION

CVD is a significant complication of MASLD. Several studies have demonstrated that patients with MASLD are at increased risk of hypertension, atherosclerosis, myocardial infarction, stroke, and chronic kidney disease.[20–23] However, the mechanism(s) by which MASLD drives the development of CVD is(are) not known. Hepatic steatosis is often associated with a cluster of other metabolic diseases such as obesity and Type II diabetes, thus, it has been difficult to determine the specific effects of hepatic steatosis on the development of CVD due to the confounding effects of obesity and associated metabolic abnormalities that often accompany MASLD. We have recently described that hepatocyte-specific PPARα knockout mice (*Ppara*[HepKO]) develop hepatic steatosis and several signs
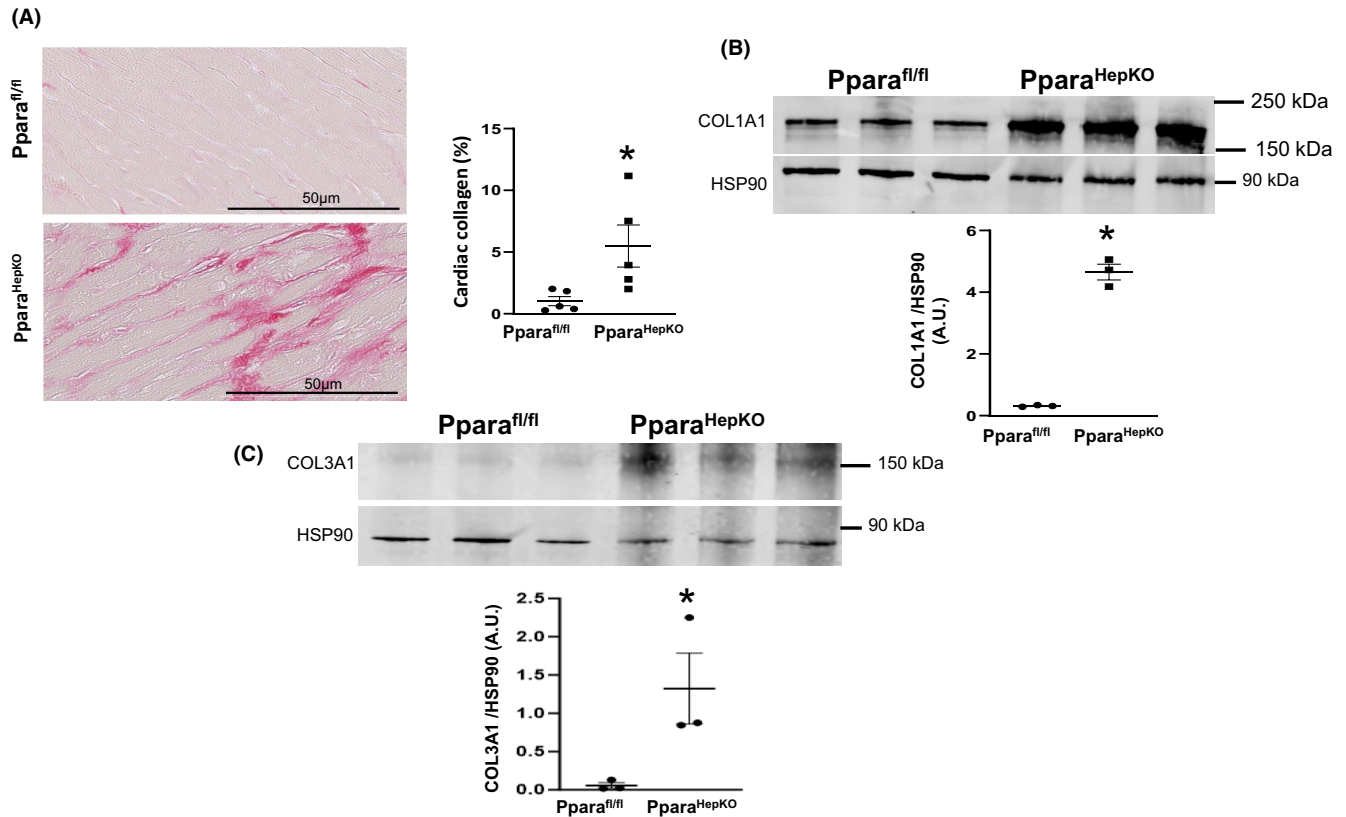
FIGURE 3 Cardiac collagen deposition in *Ppara*[HepKO] and *Ppara*^{fl/fl} mice. (A) Representative image of Picrosirius Red staining of cardiac tissue from *Ppara*[HepKO] and floxed littermate controls (*Ppara*^{fl/fl}) mice, (B) representative western bot of cardiac COL1A1 normalized to HSP90 levels and (C) cardiac COL3A1 in *Ppara*[HepKO] and *Ppara*^{fl/fl} mice. Values are expressed as means ± SEM; *$p < 0.05$ versus *Ppara*^{fl/fl}. (A) $n = 5$/group; (B and C) $n = 3$/group; Scale bar = 50 μm. COL1A1, collagen type 1 alpha 1; COL3A1, collagen type 3 alpha 1; HSP90, heat shock protein 90. Ppara^{fl/fl}, hepatocyte-specific peroxisome proliferator-activated receptor alpha flox/flox; Ppara[HepKO], hepatocyte-specific peroxisome proliferator-activated receptor alpha knockout; SEM, standard error of mean.

of CVD even when fed a normal fat diet and maintaining normal body weight and absence of Type II diabetes and increased plasma triglycerides.[13] These mice offer the opportunity to study the impact of hepatic steatosis on development of CVD independent of other metabolic diseases such as obesity and Type II diabetes. In the present study, we observed increased cardiac lipid accumulation and cell death in *Ppara*[HepKO] mice. This was accompanied by upregulated cardiac production of ANP and BNP, increased extracellular matrix remodeling, cardiomyocyte contractile dysfunction, downregulation of cardiac BDH1, and poor exercise tolerance.

Ppara[HepKO] mice exhibited significantly increased levels of cardiac steatosis and apoptosis, suggestive of lipotoxicity. Excessive lipid uptake by the heart has been linked to ventricular contractile dysfunction and impaired regulation of cardiac output.[24,25] Previous studies have also demonstrated that patients with elevated cardiac lipids exhibit systolic dysfunction similar to that observed in *Ppara*[HepKO] mice.[26,27] There is mounting evidence showing that excessive cardiac lipid accumulation causes cardiac cells to undergo programmed cell death and contribute to

heart failure.[28] In the present study, we observed increased expression of cleaved caspase 3 and pro-caspase-3, makers of programmed cell death in hearts of *Ppara*[HepKO] mice. Cleaved caspase-3 is a death-driving cysteine protease that propagates apoptotic signals.[29] Likewise, we observed an increase expression of BAX in the heart of *Ppara*[HepKO] mice. BAX is a proapoptotic protein that acts by causing mitochondrial damage and release of cytochrome *c*. The levels of the antiapoptotic protein, BCL-2, were decreased in hearts of *Ppara*[HepKO] mice suggesting a shift in the balance of pro- and antiapoptotic proteins. These results demonstrate that lipid-induced cardiomyocyte apoptosis may be a mechanism for the deterioration of cardiac function observed in *Ppara*[HepKO] mice. To the best of our knowledge, these are the first data to demonstrate a link between hepatic PPARα deficiency, increased hepatic steatosis, and cardiac lipotoxicity.

We previously showed that *Ppara*[HepKO] mice exhibit cardiac remodeling, and this is associated with increased dilation of the left ventricular chamber and wall thinning.[13] Similarly, Pattar et al. reported that ventricular remodeling and worsening of heart function is associated
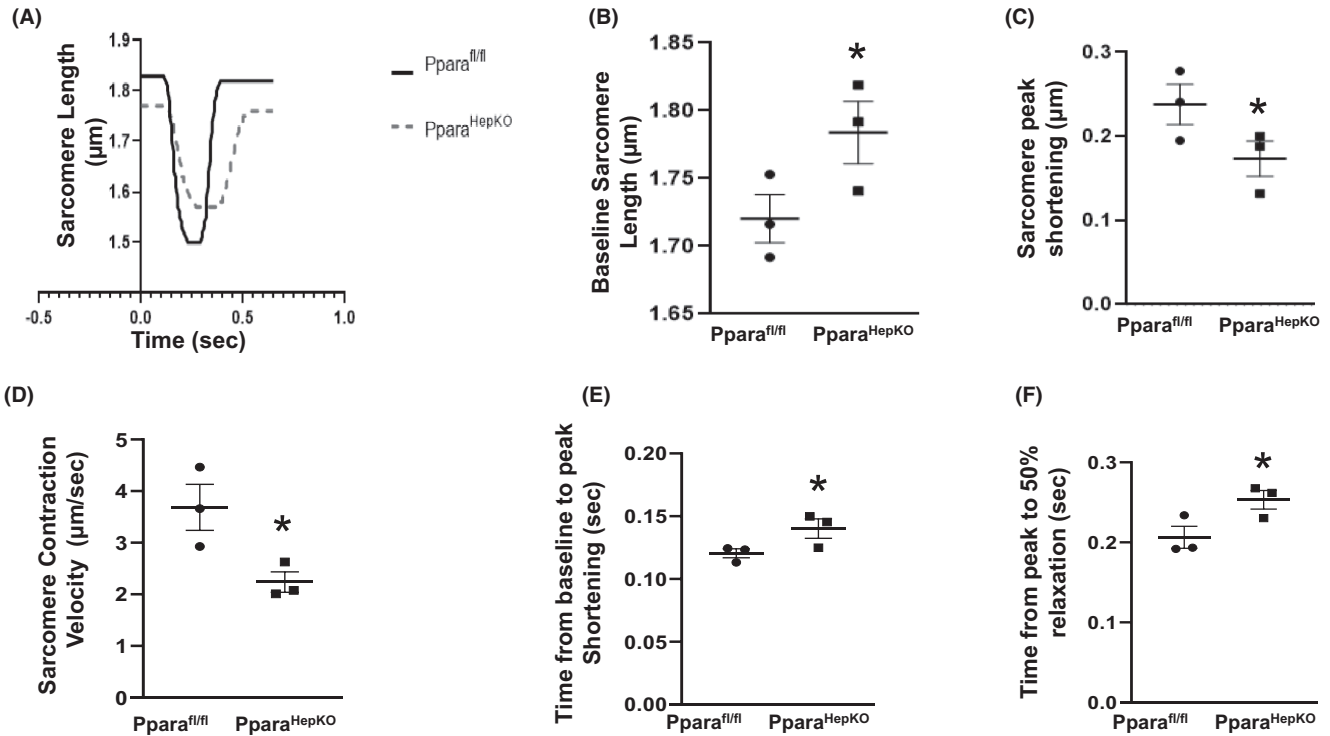
FIGURE 4 Isolated cardiomyocyte length measurement and contractile function in $Ppara^{HepKO}$ and $Ppara^{fl/fl}$ mice. (A) Representative traces of cardiomyocyte contraction/relaxation cycle, (B) baseline sarcomere length, (C) sarcomere peak shortening, (D) sarcomere contraction velocity, and (E) time from baseline to peak shortening, (F) time from peak to 50% relaxation. Values are expressed as means ± SEM; *$p < 0.05$ versus $Ppara^{fl/fl}$; $n = 30$ cardiomyocytes from three mice per group. Ppara$^{fl/fl}$, hepatocyte-specific peroxisome proliferator-activated receptor alpha flox/flox; Ppara^{HepKO}, hepatocyte-specific peroxisome proliferator-activated receptor alpha knockout; SEM, standard error of mean.

with myocardial fibrosis, wall thinning, and left ventricular dilation in ischemic injury.[30] Improper deposition of collagen and extracellular matrix within the heart contributes to the process of cardiac remodeling associated with alteration in cardiac contractility and relaxation.[31] In the present study, we observed cardiac fibrosis as evidenced by increased collagen type I and III in the heart of $Ppara^{HepKO}$ mice. Collagen type I and III are the primary extracellular matrices providing structural support to the heart.[32] The increased deposition of extracellular matrix within the interstitium leads to cardiac remodeling and stiffening of the left ventricular wall, contributing to left ventricular systolic and diastolic dysfunction.[33] There is mounting evidence that accumulation of extracellular matrix within the myocardium is a good biomarker of myocardial fibrosis.[34] Unfortunately, there are no current therapies for slowing or reversing cardiac fibrosis. Our observations suggest that cardiac remodeling coupled with ventricular diastolic dysfunction could be due to excess collagen deposition in the heart of $Ppara^{HepKO}$ mice. In the present study, we also observed contractile dysfunction in isolated cardiomyocytes of $Ppara^{HepKO}$ mice. We identified increased time from baseline to peak sarcomere shortening indicating not only impaired cardiomyocyte

contractility in $Ppara^{HepKO}$ mice but also reduced velocity of contraction when compared to $Ppara^{fl/fl}$ mice. Similarly, we observed increased time from peak to 50% relaxation, suggesting impaired cardiomyocyte relaxation. These results suggest that fibrosis of the myocardium is not the only contributor of impaired contractile function in this model, and that alterations in the contractile apparatus itself may also contribute overall cardiac dysfunction observed in $Ppara^{HepKO}$ mice.

Natriuretic hormones (ANP and BNP) are secreted from the heart in response to increased stretch. ANP is mainly secreted from the right atrium in response to atrial stretch but can also be secreted from the ventricles of patients with heart failure,[35] whereas BNP is secreted from the ventricles in response to hypervolemia and pressure overload.[36] In our earlier study,[13] we found increased end-diastolic volume in $Ppara^{HepKO}$ mice, and the resulting left ventricular overload could stretch ventricular muscles promoting increased release of ANP and BNP as demonstrated in the present study. The release of natriuretic hormones are increased in hypertensive heart and heart failure, and their elevated levels have been used as diagnostic biomarkers of heart failure.[37,38] Previous studies suggest that synthesis of elevated natriuretic peptides in
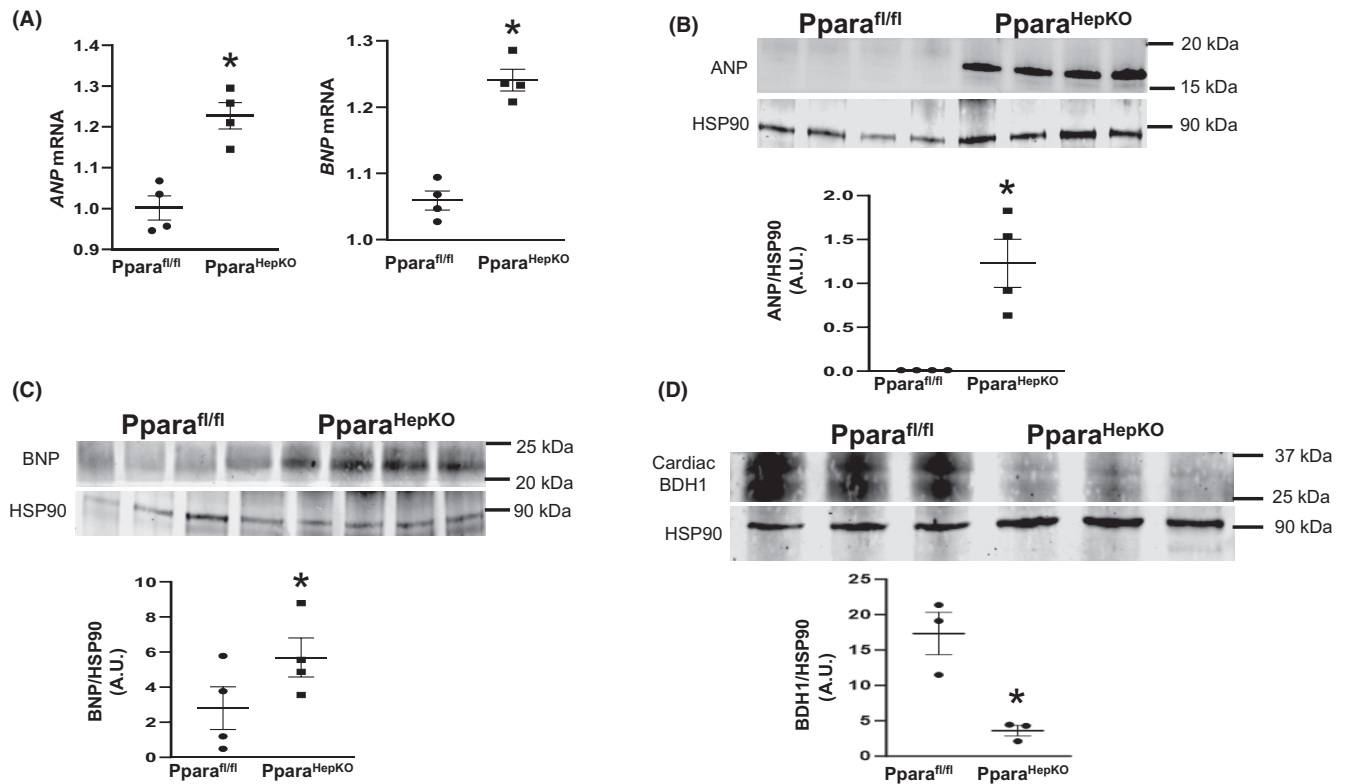
FIGURE 5 Elevated cardiac natriuretic peptide and reduced hepatic and cardiac BDH1 in *Ppara*^HepKO^ and *Ppara*^fl/fl^ mice. (A) Cardiac *ANP* and BNP mRNA levels as measured by real-time PCR, (B) representative western blot of cardiac ANP normalized to HSP90 levels, (C) representative western blot of cardiac BNP normalized to HSP90 levels, (D) representative western blot of cardiac BDH1 normalized to HSP90. Values are expressed as means $\pm$ SEM; *$p < 0.05$ versus *Ppara*^fl/fl^; (A–C) $n = 4$/group; (D) $n = 3$/group. ANP, atrial natriuretic peptide; BNP, B-type natriuretic peptide; BDH1, D-β-hydroxybutyrate dehydrogenase I; HSP90, heat shock protein 90; mRNA, messenger ribonucleic acid; PCR, polymerase chain reaction; Ppara^fl/fl^, hepatocyte-specific peroxisome proliferator-activated receptor alpha flox/flox; Ppara^HepKO^, hepatocyte-specific peroxisome proliferator-activated receptor alpha knockout; SEM, standard error of mean.

conditions of heart failure may exert a cardioprotective role by increasing vasodilation and regulating sodium-water excretion.[39] ANP and BNP can also attenuate cardiac fibrosis by regulating the renin-angiotensin-aldosterone system.[40] Thus, elevated levels of natriuretic hormones observed in the present study may help mitigate some of the increased cardiac fibrosis in *Ppara*^HepKO^ mice.

Graded maximal exercise test remains a non-invasive standard test to assess cardiovascular fitness,[41] and the VO$_{2max}$ utilized by the body during exercise is often used as an indicator of cardiovascular fitness.[42] At peak oxygen consumption, VO$_{2max}$ cannot increase further despite an increase in workload resulting in less distribution of oxygen to the tissues. Earlier studies have shown that low VO$_{2max}$, indicating poor cardiovascular fitness, has been observed in subjects with heart failure, hypertension, and diabetes.[43,44] RER, a ratio of the VCO$_2$ by VO$_2$ reflects substrate utilization by the body. The value of RER during intense exercise demonstrates whether the body is working aerobically or anaerobically. Studies have shown resting RER values between 0.7–0.8; however, during exercise or stress test, RER gradually increases to about 1.2.[44] When

RER values cross the 1.0 mark, they indicate the body has switched to anaerobic respiration (anaerobic threshold) and the VCO$_2$ at that point begins to exceed VO$_2$ to reduce blood acidity by getting rid of lactate accumulation.[45] In the present study, we observed reduced exercise performance and reduced running time to reach exhaustion *Ppara*^HepKO^ mice when compared to *Ppara*^fl/fl^ controls. Furthermore, we observed low VO$_2$ max, and reduced time needed for RER to surpass the 1.0 mark in *Ppara*^HepKO^ compared to *Ppara*^fl/fl^ mice. The reduced time needed for RER to reach the anaerobic threshold in *Ppara*^HepKO^ mice reveals the switch to the less effective anaerobic pathway earlier during the exercise test than in *Ppara*^fl/fl^ mice. Resting lactate levels were also significantly higher in *Ppara*^HepKO^ mice compared to controls. An increase in blood lactate levels has been observed in disease-induced pathophysiological stress conditions such as liver failure and heart disease.[46,47] Elevated lactate levels were documented at rest in patients with heart failure and it has been used as an independent predictor of mortality in these patients.[48,49] It is possible that reduced cardiac output previously observed in *Ppara*^HepKO^ mice might underlie the development of
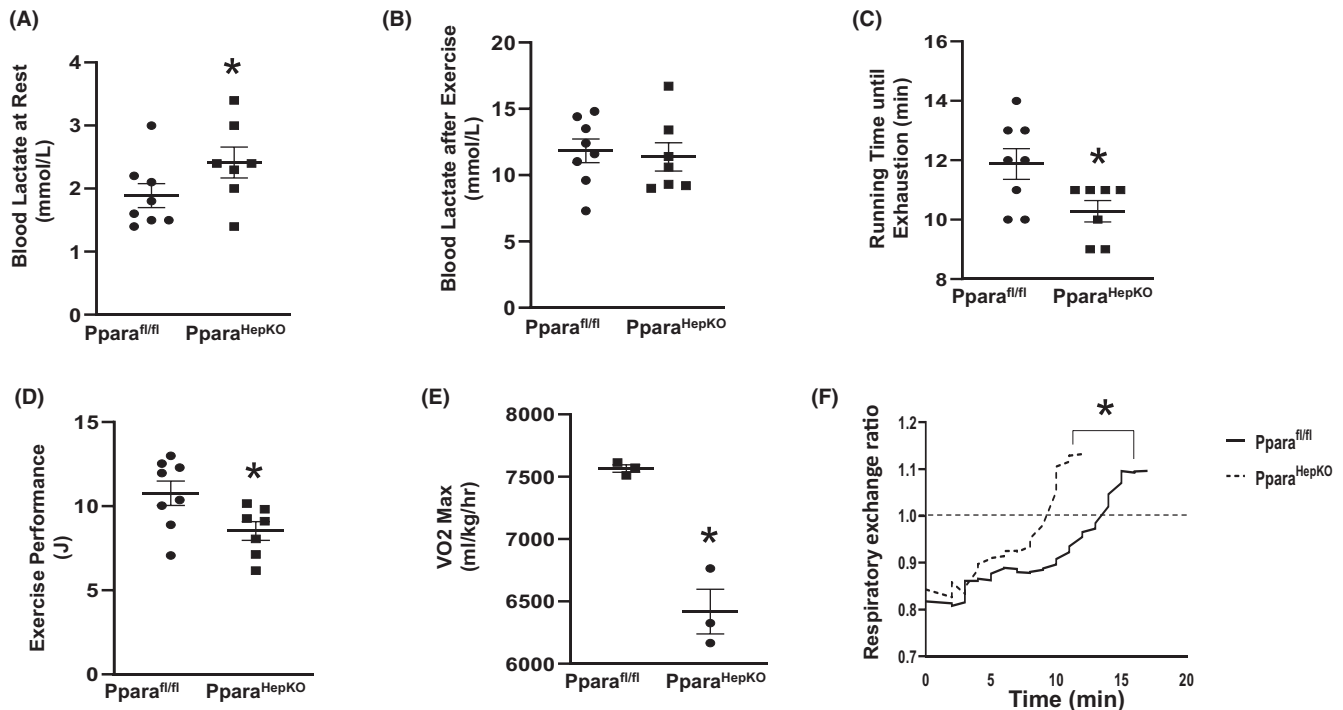
FIGURE 6 Exercise capacity test in $Ppara^{HepKO}$ and $Ppara^{fl/fl}$ mice. (A) Blood lactate at rest, (B) blood lactate after exercise, (C) running time until exhaustion, (D) exercise performance, (E) VO$_{2max}$, and (F) respiratory exchange ratio. Values are expressed as means ± SEM; *$p < 0.05$ versus $Ppara^{fl/fl}$; (A–D) $n = 7$–8/group; (E and F) $n = 3$/group. Ppara$^{fl/fl}$, hepatocyte-specific peroxisome proliferator-activated receptor alpha flox/flox; Ppara^{HepKO}, hepatocyte-specific peroxisome proliferator-activated receptor alpha knockout; SEM, standard error of mean; VO$_{2max}$, maximum volume of oxygen consumption.

hyperlactatemia as inadequate cardiac output would fail to supply enough oxygen to the tissues resulting in hypoxia and lactate build-up through anaerobic respiration via the pyruvic pathway. It has been previously demonstrated that lactate is a fuel substrate for the failing heart, and in the incidence of hyperlactatemia, lactate may supply up to 60% of fuel substrate to the heart.[50] The heart, which is one of the most energy demanding organs in the body, normally uses fatty acid oxidation as the principal source of ATP production but it can switch between other substrates (glucose, lactate, and ketone) to generate ATP when necessary. Usually, during pathological conditions, the heart utilizes ketone as fuel substrate to maintain cardiac energy metabolism.[51] It is also possible that the elevation in resting lactate levels observed in the Ppara^{HEPKO} mice are due to suppression of pyruvate dehydrogenase as a result of the Randle cycle; however, this hypothesis needs to be further tested.[52]

In our previous work, we observed reduced circulating beta hydroxybutyrate (BHOB), the most abundant ketone body, in $Ppara^{HepKO}$ mice.[13] BDH1 is the rate-limiting enzyme that converts acetoacetate to BHOB in the liver before entering the circulation. Similarly, BDH1 in the heart catalyzes the conversion of BHOB back to acetoacetate to supply the heart with ATP.[53] Our present data revealed reduced cardiac BDH1 in $Ppara^{HepKO}$ mice, suggesting reduced

ketones production in the liver and reduced ketones utilization by the heart. While a shift in energy substrate from fatty acid oxidation to ketones in failing heart has been described, our data is the first to report that cardiac BHOB utilization is reduced in animals lacking PPARα in hepatocytes. Rosenstein and Hough[54] reported that an increased reliance of the failing heart on ketones can improve heart function whereas failure to use ketones by a failing heart is associated with worse outcomes. Taken together, our results in combination with these previous studies support the hypothesis that the failing heart may be further compromised by reduced BHOB utilization. Our results also suggest that due to reduced cardiac ketones utilization, the heart may be reprogramed to increase utilization of lactate as an energy substrate in $Ppara^{HepKO}$ mice.

Our results demonstrate that hepatic steatosis induced by loss of hepatic PPARα results in excess cardiac lipid accumulation, cardiomyocyte apoptosis, increased collagen deposition, deficits in cardiac myocyte contractility, impaired VO$_{2max}$ during exercise, and reduced BDH1 levels leading to impaired functionality of the heart. In addition, we further demonstrate that the $Ppara^{HepKO}$ mouse model may be an important tool to investigate the mechanisms by which hepatic steatosis affects cardiac structure and function in the absence of other confounding factors associated with obese and metabolic syndrome and may also be

a useful model for development of new therapeutic targets for the cardiac complications of MASLD.

CONFLICT OF INTEREST STATEMENT
No conflicts of interest, financial or otherwise, are declared by the authors.

DATA AVAILABILITY STATEMENT
The data that support the findings of this study are available in the results of this article. Original data of any additional information that support the findings of this study will be available on request from the corresponding author.

ORCID
Olufunto O. Badmus https://orcid.org/0000-0002-1020-2170
Alexandre A. da Silva https://orcid.org/0000-0003-4504-0607
David E. Stec https://orcid.org/0000-0001-8359-4008
Lucy C. Taylor https://orcid.org/0009-0009-9267-6713

REFERENCES
1. Przybyszewski EM, Targher G, Roden M, Corey KE. Nonalcoholic fatty liver disease and cardiovascular disease. *Clin Liver Dis (Hoboken)*. 2021;17(1):19-22.

2. Badmus OO, Hinds TD Jr, Stec DE. Mechanisms linking metabolic-associated fatty liver disease (MAFLD) to cardiovascular disease. *Curr Hypertens Rep*. 2023;25(8):151-162.

3. Rinella ME, Lazarus JV, Ratziu V, et al. A multi-society Delphi consensus statement on new fatty liver disease nomenclature. *Hepatology*. 2023;79:E93-E94.

4. Niederseer D, Wernly B, Aigner E, Stickel F, Datz C. NAFLD and cardiovascular diseases: epidemiological, mechanistic and therapeutic considerations. *J Clin Med*. 2021;10(3):467.

5. Arroyave-Ospina JC, Wu Z, Geng Y, Moshage H. Role of oxidative stress in the pathogenesis of non-alcoholic fatty liver disease: implications for prevention and therapy. *Antioxidants (Basel)*. 2021;10(2):174.

6. Creeden JF, Gordon DM, Stec DE, Hinds TD Jr. Bilirubin as a metabolic hormone: the physiological relevance of low levels. *Am J Physiol Endocrinol Metab*. 2021;320(2):E191-E207.

7. Gambino R, Bugianesi E, Rosso C, et al. Different serum free fatty acid profiles in NAFLD subjects and healthy controls after Oral fat load. *Int J Mol Sci*. 2016;17(4):479.

8. Zhang QQ, Lu LG. Nonalcoholic fatty liver disease: dyslipidemia, risk for cardiovascular complications, and treatment strategy. *J Clin Transl Hepatol*. 2015;3(1):78-84.

9. Montgomery MK, De Nardo W, Watt MJ. Impact of lipotoxicity on tissue "cross talk" and metabolic regulation. *Physiology (Bethesda)*. 2019;34(2):134-149.

10. Drosatos K, Schulze PC. Cardiac lipotoxicity: molecular pathways and therapeutic implications. *Curr Heart Fail Rep*. 2013;10(2):109-121.

11. Unger RH, Orci L. Lipotoxic diseases of nonadipose tissues in obesity. *Int J Obes Relat Metab Disord*. 2000;24(Suppl 4):S28-S32.

12. Goldberg IJ, Trent CM, Schulze PC. Lipid metabolism and toxicity in the heart. *Cell Metab*. 2012;15(6):805-812.

13. Badmus OO, Kipp ZA, Bates EA, et al. Loss of hepatic PPARalpha in mice causes hypertension and cardiovascular disease. *Am J Physiol Regul Integr Comp Physiol*. 2023;325(1):R81-R95.

14. Stec DE, Gordon DM, Hipp JA, et al. Loss of hepatic PPARalpha promotes inflammation and serum hyperlipidemia in diet-induced obesity. *Am J Physiol Regul Integr Comp Physiol*. 2019;317(5):R733-R745.

15. Hinds TD Jr, Burns KA, Hosick PA, et al. Biliverdin reductase a attenuates hepatic steatosis by inhibition of glycogen synthase kinase (GSK) 3beta phosphorylation of serine 73 of peroxisome proliferator-activated receptor (PPAR) alpha. *J Biol Chem*. 2016;291(48):25179-25191.

16. Hinds TD Jr, Creeden JF, Gordon DM, Stec DF, Donald MC, Stec DE. Bilirubin nanoparticles reduce diet-induced hepatic steatosis, improve fat utilization, and increase plasma beta-Hydroxybutyrate. *Front Pharmacol*. 2020;11:594574.

17. Schipke J, Brandenberger C, Rajces A, et al. Assessment of cardiac fibrosis: a morphometric method comparison for collagen quantification. *J Appl Physiol (1985)*. 2017;122(4):1019-1030.

18. Kipp ZA, Martinez GJ, Bates EA, et al. Bilirubin nanoparticle treatment in obese mice inhibits hepatic ceramide production and remodels liver fat content. *Metabolites*. 2023;13(2):215.

19. Li X, Flynn ER, do Carmo JM, et al. Direct cardiac actions of sodium-glucose cotransporter 2 inhibition improve mitochondrial function and attenuate oxidative stress in pressure overload-induced heart failure. *Front Cardiovasc Med*. 2022;9:859253.

20. Adams LA, Anstee QM, Tilg H, Targher G. Non-alcoholic fatty liver disease and its relationship with

cardiovascular disease and other extrahepatic diseases. *Gut*. 2017;66(6):1138-1153.

21. Aneni EC, Oni ET, Martin SS, et al. Blood pressure is associated with the presence and severity of nonalcoholic fatty liver disease across the spectrum of cardiometabolic risk. *J Hypertens*. 2015;33(6):1207-1214.

22. Brea A, Mosquera D, Martin E, Arizti A, Cordero JL, Ros E. Nonalcoholic fatty liver disease is associated with carotid atherosclerosis: a case-control study. *Arterioscler Thromb Vasc Biol*. 2005;25(5):1045-1050.

23. Park H, Dawwas GK, Liu X, Nguyen MH. Nonalcoholic fatty liver disease increases risk of incident advanced chronic kidney disease: a propensity-matched cohort study. *J Intern Med*. 2019;286(6):711-722.

24. Hu C, Ge F, Hyodo E, et al. Chronic ethanol consumption increases cardiomyocyte fatty acid uptake and decreases ventricular contractile function in C57BL/6J mice. *J Mol Cell Cardiol*. 2013;59:30-40.

25. Yagyu H, Chen G, Yokoyama M, et al. Lipoprotein lipase (LpL) on the surface of cardiomyocytes increases lipid uptake and produces a cardiomyopathy. *J Clin Invest*. 2003;111(3):419-426.

26. Szczepaniak LS, Dobbins RL, Metzger GJ, et al. Myocardial triglycerides and systolic function in humans: in vivo evaluation by localized proton spectroscopy and cardiac imaging. *Magn Reson Med*. 2003;49(3):417-423.

27. Mahmod M, Bull S, Suttie JJ, et al. Myocardial steatosis and left ventricular contractile dysfunction in patients with severe aortic stenosis. *Circ Cardiovasc Imaging*. 2013;6(5):808-816.

28. Sparagna GC, Hickson-Bick DL. Cardiac fatty acid metabolism and the induction of apoptosis. *Am J Med Sci*. 1999;318(1):15-21.

29. Bell RAV, Megeney LA. Evolution of caspase-mediated cell death and differentiation: twins separated at birth. *Cell Death Differ*. 2017;24(8):1359-1368.

30. Pattar SS, Fatehi Hassanabad A, Fedak PWM. Acellular extracellular matrix bioscaffolds for cardiac repair and regeneration. *Front Cell Dev Biol*. 2019;7:63.

31. Cowling RT, Kupsky D, Kahn AM, Daniels LB, Greenberg BH. Mechanisms of cardiac collagen deposition in experimental models and human disease. *Transl Res*. 2019;209:138-155.

32. Singh D, Rai V, Agrawal DK. Regulation of collagen I and collagen III in tissue injury and regeneration. *Cardiol Cardiovasc Med*. 2023;7(1):5-16.

33. Frangogiannis NG. Cardiac fibrosis. *Cardiovasc Res*. 2021;117(6):1450-1488.

34. Wight TN, Potter-Perigo S. The extracellular matrix: an active or passive player in fibrosis? *Am J Physiol Gastrointest Liver Physiol*. 2011;301(6):G950-G955.

35. Lee NS, Daniels LB. Current understanding of the compensatory actions of cardiac natriuretic peptides in cardiac failure: a clinical perspective. *Card Fail Rev*. 2016;2(1):14-19.

36. Oremus M, McKelvie R, Don-Wauchope A, et al. A systematic review of BNP and NT-proBNP in the management of heart failure: overview and methods. *Heart Fail Rev*. 2014;19(4):413-419.

37. Kessler-Icekson G, Barhum Y, Schaper J, Schaper W, Kaganovsky E, Brand T. ANP expression in the hypertensive heart. *Exp Clin Cardiol*. 2002;7(2–3):80-84.

38. Ibrahim NE, Januzzi JL Jr. Established and emerging roles of biomarkers in heart failure. *Circ Res*. 2018;123(5):614-629.

39. Kuwahara K. The natriuretic peptide system in heart failure: diagnostic and therapeutic implications. *Pharmacol Ther*. 2021;227:107863.

40. Kerkela R, Ulvila J, Magga J. Natriuretic peptides in the regulation of cardiovascular physiology and metabolic events. *J Am Heart Assoc*. 2015;4(10):e002423.

41. Moreno-Cabanas A, Ortega JF, Morales-Palomo F, et al. The use of a graded exercise test may be insufficient to quantify true changes in V̇o(2max) following exercise training in unfit individuals with metabolic syndrome. *J Appl Physiol (1985)*. 2020;129(4):760-767.

42. Poole DC, Wilkerson DP, Jones AM. Validity of criteria for establishing maximal O_2 uptake during ramp exercise tests. *Eur J Appl Physiol*. 2008;102(4):403-410.

43. Sawada S, Tanaka H, Funakoshi M, Shindo M, Kono S, Ishiko T. Five year prospective study on blood pressure and maximal oxygen uptake. *Clin Exp Pharmacol Physiol*. 1993;20(7–8):483-487.

44. Leite SA, Monk AM, Upham PA, Bergenstal RM. Low cardiorespiratory fitness in people at risk for type 2 diabetes: early marker for insulin resistance. *Diabetol Metab Syndr*. 2009;1(1):8.

45. Myers J, Ashley E. Dangerous curves. A perspective on exercise, lactate, and the anaerobic threshold. *Chest*. 1997;111(3):787-795.

46. Murphy ND, Kodakat SK, Wendon JA, et al. Liver and intestinal lactate metabolism in patients with acute hepatic failure undergoing liver transplantation. *Crit Care Med*. 2001;29(11):2111-2118.

47. Gjesdal G, Braun OO, Smith JG, Schersten F, Tyden P. Blood lactate is a predictor of short-term mortality in patients with myocardial infarction complicated by heart failure but without cardiogenic shock. *BMC Cardiovasc Disord*. 2018;18(1):8.

48. Ander DS, Jaggi M, Rivers E, et al. Undetected cardiogenic shock in patients with congestive heart failure presenting to the emergency department. *Am J Cardiol*. 1998;82(7):888-891.

49. Kawase T, Toyofuku M, Higashihara T, et al. Validation of lactate level as a predictor of early mortality in acute decompensated heart failure patients who entered intensive care unit. *J Cardiol*. 2015;65(2):164-170.

50. Lazzeri C, Valente S, Chiostri M, Gensini GF. Clinical significance of lactate in acute cardiac patients. *World J Cardiol*. 2015;7(8):483-489.

51. Horton JL, Davidson MT, Kurishima C, et al. The failing heart utilizes 3-hydroxybutyrate as a metabolic stress defense. *JCI Insight*. 2019;4(4):e124079.

52. Hue L, Taegtmeyer H. The randle cycle revisited: a new head for an old hat. *Am J Physiol Endocrinol Metab*. 2009;297(3):E578-E591.

53. Newman JC, Verdin E. Beta-Hydroxybutyrate: a signaling metabolite. *Annu Rev Nutr*. 2017;37:51-76.

54. Rosenstein R, Hough A. Empagliflozin, cardiovascular outcomes, and mortality in type 2 diabetes. *N Engl J Med*. 2016;374(11):1093-1094.